ORIGINAL PAPER

Accurate determination of the Taşkent (Konya, Turkey) landslide using a long-range terrestrial laser scanner

M. Zeybek · İ. Şanlıoğlu

Abstract Landslides are a common type of mass movement that occur in large numbers and have significant effects on topography. In Turkey, landslides rank second after earthquakes among natural disasters that cause widespread loss of life and property. This study investigates the monitoring of the Taşkent Landslide (Konya, Turkey), which has considerably affected the local topography. The landslide in Taşkent had an adverse effect on transportation to nearby towns and villages. Initial studies were conducted using the global navigation satellite system (GNSS) measurement scale; these studies are currently ongoing. Since 2011, studies using terrestrial laser scanning (TLS), which is one of the latest ground-positioning technologies, have also been launched. This article presents the results of the TLS and GNSS approaches used to monitor, characterise and model an active landslide. It includes the comparison and analysis of a point cloud, three-dimensional model, profile and change in volume mass acquired in different time periods in one landslide area. The point cloud data, obtained from two different time periods using the TLS technique, and supported by the results of GNSS analysis, were analysed via different methods. The TLS revealed that up to 4 m of material was displaced at the site of the landslide, and it revealed detailed information about how the landslide occurred. The volume of the mass that moved as a result of the landslide was determined, and movements that occurred in the geological structure were monitored. These studies showed that the TLS point cloud method can be effectively used in the monitoring of landslides that occur in areas that are large, difficult to reach, rugged or mountainous.

Keywords Taşkent · Terrestrial laser scanner · Landslide · Monitoring

Introduction

Landslides pose a serious and considerable danger in areas that are rugged, sloping or mountainous. In addition to posing a constant threat to the lives of people who live in these areas, landslides can also cause considerable damage to man-made structures such as roads, dams, substructure systems, electric lines, telephone lines and works of art.

Many scientists have conducted studies on landslides and continue to do so today (Brideau et al. 2012). Abellán et al. (2006) carried out studies on rock falls using the long-range laser scanning method. From the extensive data obtained from these studies, highly accurate digital elevation models and geometries were created. Teza et al. (2007) produced detailed digital models and prepared reliable displacement maps using data provided by terrestrial laser scanning (TLS) observations through both the implementation of multiple TLS sessions on landslide surfaces and the assistance of multi-time interferometric synthetic aperture radar (INSAR) observations. Thus, the researchers were able to make comparisons between the INSAR and TLS techniques. Teza et al. (2008a) also obtained displacement vectors by conducting multiple observations with TLS and calculated the stress fields based on these vectors. In recent years, the use of TLS in deformation measurements has increased. Monserrat and Crosetto (2008), for example, conducted studies on deformations and ground movements using repeated TLS scans. In their

M. Zeybek (✉) · İ. Şanlıoğlu
University of Selcuk, Konya, Turkey
e-mail: mzeybek@selcuk.edu.tr

İ. Şanlıoğlu
e-mail: sanlioglu@selcuk.edu.tr

study, the authors made use of the least-squares three-dimensional (3D) surface matching method, which was developed by Gruen and Akca (2005). Casula et al. (2010) conducted research on the potential reliability of the integration of the global navigation satellite system (GNSS), TLS and total stations in geomorphological studies.

Several assessments have been made using TLS data in rocky, high-risk areas. It has been shown that a high-precision TLS technique is an appropriate support system in cases of emergency, protection and land management (Fanti et al. 2012; Gigli et al. 2012; Viero et al. 2012).

Numerous methods and several different sensors have been developed to investigate and monitor landslides (Travelletti et al. 2011). These monitoring techniques can be classified into two basic groups: (1) point-based techniques (the use of GNSS, extensometers, total stations, and laser and radar distance measuring equipment) and (2) surface-based techniques (photogrammetry and the use of satellite-based and ground-based radar interferometers, airborne laser scanning systems and terrestrial laser scanning systems) (Kasperski et al. 2010; Teza et al. 2007, 2008a).

Point-based measurements are more sensitive in terms of accuracy, but cannot provide information about the entirety of a landslide area. These techniques only offer information about a relevant point. In this study, however, TLS results were supported by GNSS measurements and analysis. Thus, in the results section, the advantages and disadvantages of TLS and GNSS surveys will be compared. Techniques that offer information about the surface of an area, on the other hand, can facilitate the gathering of information through distance sensing techniques, even in areas that are hard to access. These techniques have attained a high degree of accuracy as the result of advances in technology. This gradually developing technology meets the desired accuracy requirements for landslide studies (Gallay et al. 2013).

The GNSS technique has been widely implemented to monitor landslides in the last decade, both as a supplement and as an alternative to traditional surveying methods (Wang et al. 2011; Bruckl et al. 2006; Gili et al. 2000). The GNSS technique and TLS had been applied to the monitoring of the Taşkent landslide. This article presents the results obtained by using both the TLS and GNSS approaches to monitor, characterise and model an active landslide. The GNSS and TLS provided complementary measurements with the GNSS providing a point's horizontal and vertical movements and TLS providing surface motion.

This article includes the comparison and analysis of a point cloud, 3D model, profile and change-in-volume-mass results acquired in different time periods in one landslide area. While these well-known methods have been partially implemented in previous studies, this study combines TLS and GNSS results to determine the landslide side. TLS results are found to be consistent with GNSS results.

Characterisation of the study area

Location

The landslide, which occurred on slopes with elevations ranging between 1,400 m and 1,600 m in the Sazak Valley, flowed in a northerly direction. It occurred in an area covering approximately 50 ha. A 40-ha section of the landslide area included forest and farmland. The study area is approximately 10 ha in size. According to GNSS data from 2010 to 2011, the annual movement was as high as 2 m.

The landslide in question occurred between 1,000.00 km and 1,300.00 km (notation used for roads in Turkey) en route to the town of Balcılar in the Taşkent district, which is approximately 130 km from Konya and situated at the southernmost tip of the district. A site location map of the study area is shown in Fig. 1.

The elevation of the area is approximately 1,600 m above sea level. Findings obtained during fieldwork indicate that there are frequent mass movements such as landslides and rock falls in the area. The traces left by these natural disasters on the topography are visible to the naked eye, and these natural phenomena continue to alter the topography. Landslides in the area cause serious economic damage to telephone lines, roads and the sheeting and retaining walls that protect roads and agricultural activities (Fig. 2). Moreover, rock falls resulting from the geological structure of the Taşkent region are quite frequent. Rock falls also inflict significant amounts of material damage and create fear among the populace.

The road that crosses this area is a major artery that connects Taşkent to the town of Balcılar and seven other villages. Landslides damage this road every winter and sometimes block access (Fig. 3). During the summer months of 2011, the Republic of Turkey General Directorate of Highways (TCK) removed the mass that had slid over the road and installed terracing to reduce the impact of future landslides. Terracing and floating, as well as the renovation of a 300-m section of the road, cost approximately US $570,000. Our study revealed that landslides continue to occur and cannot be prevented by forming floats. An enormous debris flow that occurred following a heavy snowfall in mid-March 2012 closed the road to traffic; the road was reopened only after extensive clean-up efforts (Fig. 3).

Geology of the landslide area

In the landslide area and its vicinity, the lower layer consists of a Taşkent complex of the Upper Cretaceous Paleocene era. Above this complex layer are layers of the Mesozoic era, overlaying Korualan and Dedemli formations, and above these formations is an overlaying Zindancık complex, which is from the Triassic.
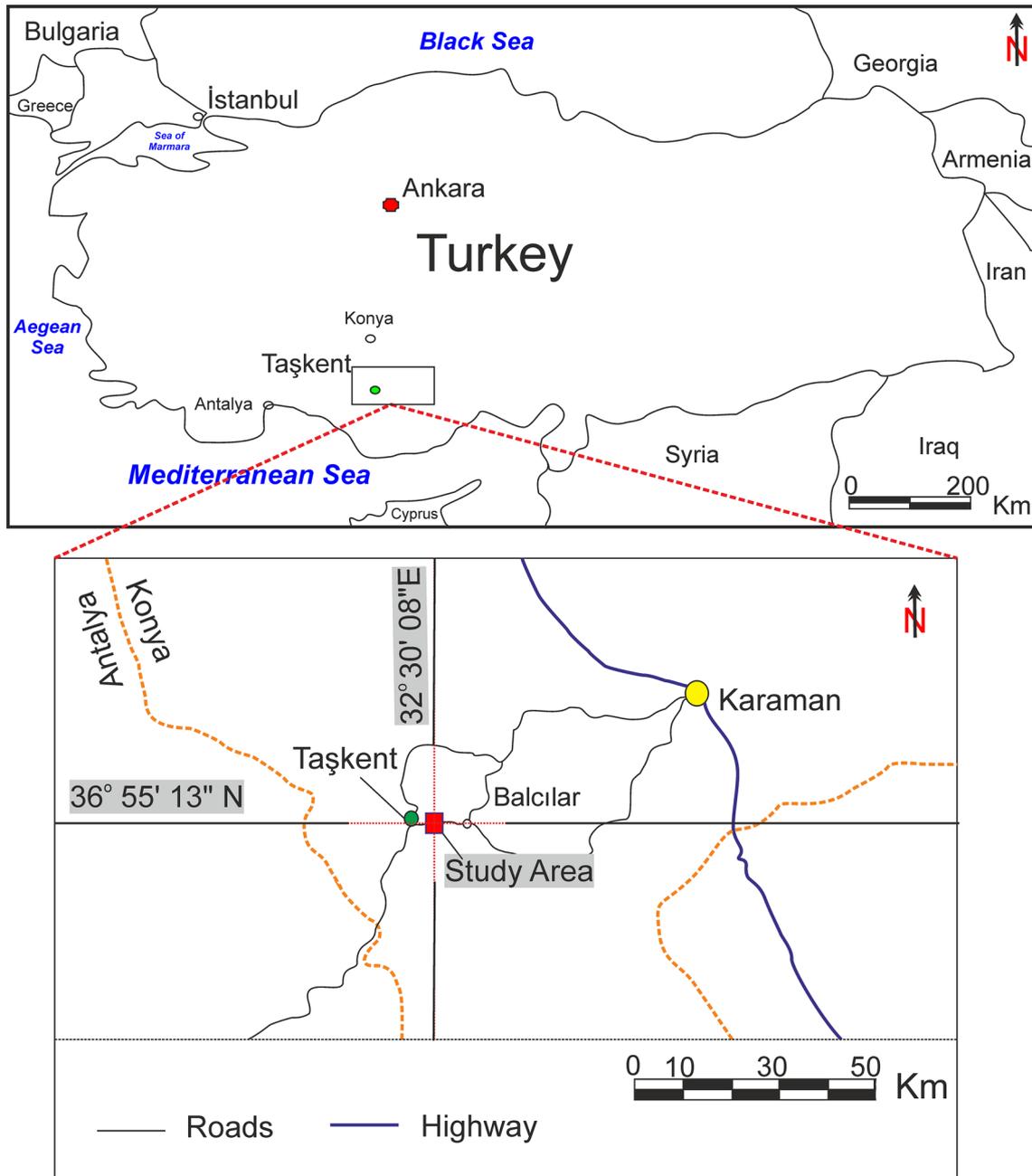
Fig. 1 Site location map of the study area

The Taşkent formation is composed of shale-intercalated marns, ophiolitic rock pieces, chert limestone and radiolarite pieces. In certain places, the formation consists of argillaceous limestone and mudstone.

The Korualan formation, which is located to the south of the landslide area, is composed of argillaceous limestone consisting of shale, limestone, sandstone, claystone and tuffite intermediate layers.

The Dedemli formation consists of sandstone, limestone, shale and volcanic sandstone, tuff and tuffite layers.

The Zindancık complex is composed of meta-shale, quartzite, meta-chert intercalation and crystallised limestone pieces. Moreover, quartzite and meta-shale in alteration zones, including crystallised limestone, slates and phyllites, are observed in this complex (Özgül 1997).

In general, the Korualan formation consists of limestone with several fractures and cracks. This formation constitutes the peak in the south of the landslide area. This formation discharges underground water through its fractures and cracks into the Sazak brook, either through springs or

Fig. 2 Effects of the Taşkent landslide on topography **a** cracks that have formed on land and telephone lines that have been damaged (*red circle*) **b** a retaining wall that has been damaged **c** a drainage ditch that has been filled with earth and become unusable **d** landslide area cracks
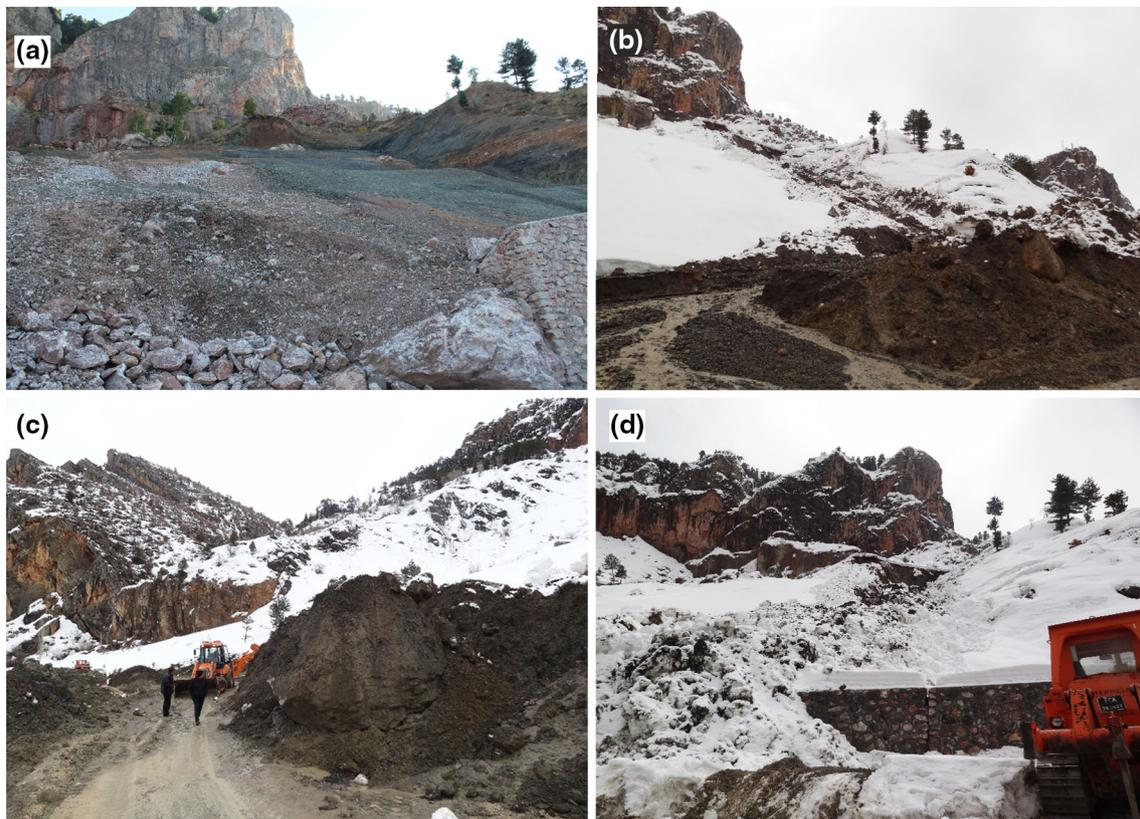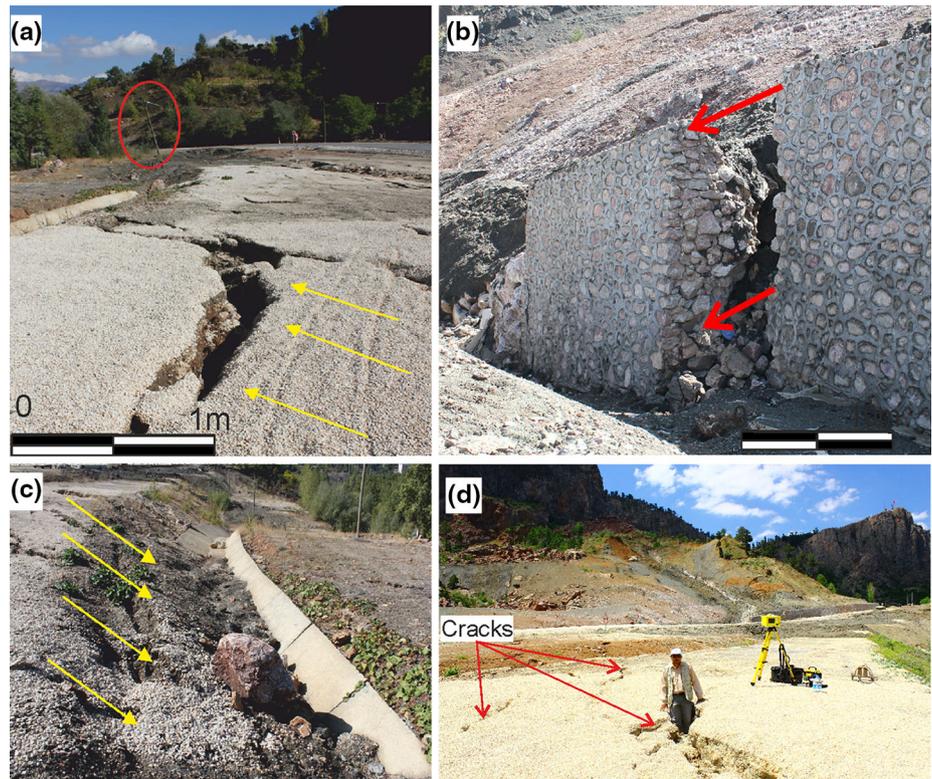

Fig. 3 a Result of floating work conducted by TCK during autumn months **b** landslide area and the earth that slid as a result of heavy snowfall **c** the large mass that slid **d** road-opening work done by bulldozers

underground leakage. The landslide area is situated between the limestone water discharge zone and the Sazak brook (Turan 2000). The landslide occurred on the ophiolites of the Taşkent formation, with cankered shale and the slope debris above them. These units are fed by underground water emanating from both the surface and the Korualan formation. The portions of ophiolites that have been weathered, degenerated and clayed in many places, as well as the saturated shales, lose their resistance, resulting in a landslide. Although underground water levels in the area where the landslide occurred vary between 11 and 19 m, these figures are lower in the winter and spring. Moreover, heavy snows are typical in this area. In spring, ample rains combine with melting snow to create a pressurised discharge of water that enters the landslide area through underground leakage. The reduced resistance of the clay, shale and slope debris is believed to be the primary reason behind the formation of the landslide. Mass movement typically occurs on the circular sliding surface.

Materials and methods

Terrestrial laser scanning technique

The use of terrestrial laser scanning is gradually increasing in the development of 3D models of large areas, especially those with a complex structure and topography (Heritage and Large 2009; Kasperski et al. 2010; Ghuffar et al. 2013; Ristic et al. 2012). The distinct disadvantage of TLS in providing positional (spatial) data is the angle of view, for which only the positional data of objects that are in the foreground are recorded (Travelletti et al. 2013; Teza et al.

2008b). As a consequence, the areas in the background cannot receive laser signals and remain shaded. The best solution to this problem is to increase the number of data points by establishing multiple stations that have different angles (Fig. 4).

A critical point to note is that each scan has its own coordinate system; therefore, there are transformations among coordinates (Kraus 2007; Pesci et al. 2011; Guarnieri et al. 2011, 2013). Dense point clouds are obtained by combining results from multiple stations in the same coordinate system, and data sets that serve as the basis for a high-resolution digital elevation model covering the entire relevant area are thus generated.

In this study, an ILRIS-3D laser scanning device was used. This device has the capacity to generate intensive point cloud data and is equipped with a unit that provides photographs. Moreover, it is equipped with a liquid–crystal-display monitor and a digital camera for online imagery. This device can be used in mining, industry, mapping and other fields of engineering. It is frequently used for dynamic measurements because it generates high-resolution and sensitive data. The device's dimensions resemble those of total stations. Because it is rather heavy (although its dimensions are typical), difficulties arise during transportation between station points. Further information can be obtained from http://www.optech.com/index.php/product/optech-ilris/. The basic parameters of the device are provided in Table 1.

Data acquisition, registration and geo-referencing

Laser scanning work was initiated at the Taşkent Landslide area in 2011 to monitor the movement of the landslide. In this study, data from measurements taken at two different
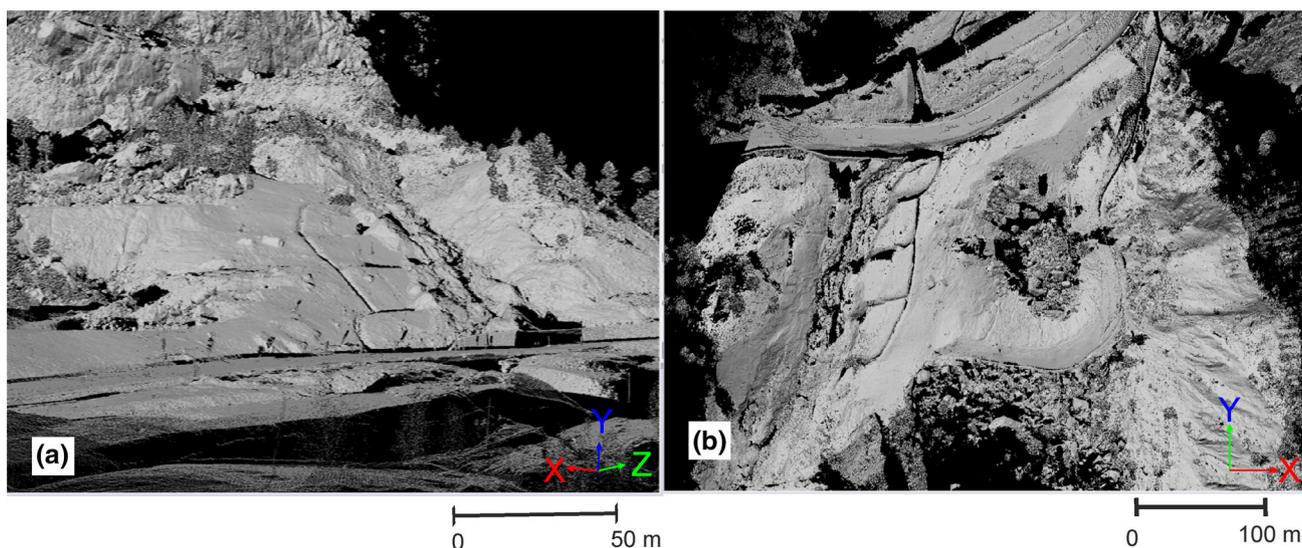

Fig. 4 a Perspective **b** view from above obtained from the intensive point cloud of the study area

Table 1 ILRIS 3D scanner features

Dynamic scanning range	3–1,500 m
Accuracy	Range: ± 7 mm at 100 m, Positional: ± 8 mm at 100 m
Sampling rate	2,000 points/seconds
Minimum spot step (X and Y axis)	0.00115°
Operation interface	Digital camera: 4 mp Viewfinder: 17 cm VGA
Controller	PDA
Size	312 × 312 × 205 mm
Operating temperature	0°–40°
Scanner field of view	40° × 40°
Eye safety laser class	Class 1 IEC 600825-1

● Scanner Positions
○ Ground Control Points

Fig. 5 Position of terrestrial laser scanning stations and locations of ground control points

times were evaluated. The first measurement was taken on November 18, 2011, and the second was taken on April 23, 2012.

To obtain data covering the entire area, measurements were made during five different sessions (Fig. 5) to prevent the formation of shaded areas (areas that would not yield data) or reduce them to a minimum. The distances between the objects and TLS were from 55 m to 200 m in scans performed at different stations. In each period, scans performed in different sessions were combined and the point clouds (whose details will be presented later) were obtained.

Scans were recorded in high-resolution mode to obtain dense point clouds. Point intervals varied between 5 cm and 10 cm, depending on the distance of the scanning. All point clouds were arranged so that they would lie on the same coordinate system. This procedure was performed

using the Iterative Closest Point (ICP) algorithm provided by the IMAlign module, which is included in Innovmetric PolyWorks software (Besl and McKay 1992). Natural points were selected on the landscape surface as tie points. Ground control points were used to ensure that the coordinates of all of the series obtained from the landscape area were on the same coordinate system (geo-referencing). For each period, the coordinates of these ground control points were defined using the global navigation satellite system–real time kinematic (GNSS–RTK) method, according to the ITRF-96 (International Terrestrial Reference Frame-96) coordinate system. The root mean square (RMS) errors for these coordinates are shown in Fig. 6.

In the GNSS–RTK measurements, the coordinates of a fixed and specific point outside the landslide area were considered to be those of a fixed station. The same fixed point was used in measurements performed in different periods. Two Javad Triumph receiving and earth antenna sets, one fixed and the other mobile, were used in these measurements. Ten-epoch coordinate data were recorded in one-second-epoch intervals. The large number of ground control points reduces referencing errors; therefore, there must be a minimum of three ground control points (Polyworks 2007). Geo-referencing was performed with four ground control points during period 1 and with six ground control points during period 2 (Fig. 5). A specially designed prismatic, reflective tinfoil material with 80 % reflection capacity was used to establish the ground control points. These points were established in cylindrical levels (tribrach) on tables (Fig. 7). Ground control points were then manually determined in point clouds for geo-referencing and converted to the ITRF-96 coordinate system (Tables 2, 3). This conversion was performed for measurements in two different periods. Thus, it was ensured that both sets of scanning data were on the same coordinate system.

Data processing and TLS accuracy

The distributions of point clouds in a virtual environment are not homogeneous; there are objects in the relevant topography that have different reflective qualities, and different point frequencies are determined at different measurement distances. Additionally, the desired quantity of data cannot be obtained in some areas because a laser beam can be refracted or reflected at different angles and absorbed. Even with proper planning at the measurement stage, there may be areas that do not yield data. Therefore, digital terrain models (DTMs) are necessary (Cavalli and Marchi 2008; Corsini et al. 2007, 2009; Daehne and Corsini 2013).

It was determined during landscape observations and GNSS studies that were previously conducted in this region

Fig. 6 RTK Solutions **a** RMS values belonging to the first period **b** RMS values belonging to the second period
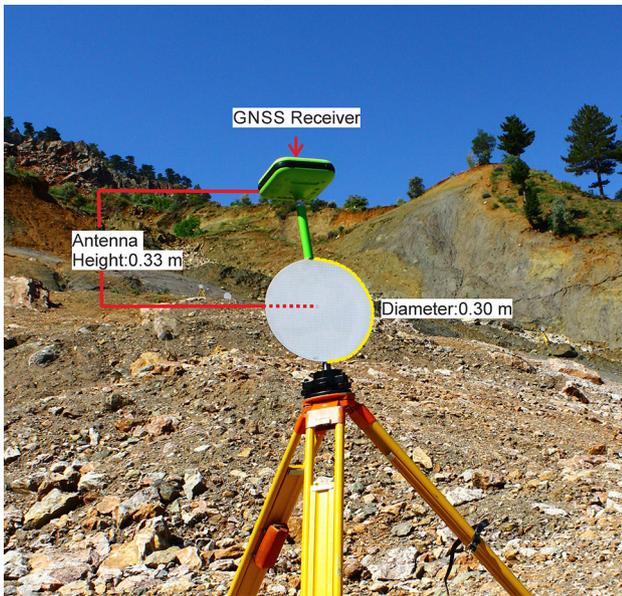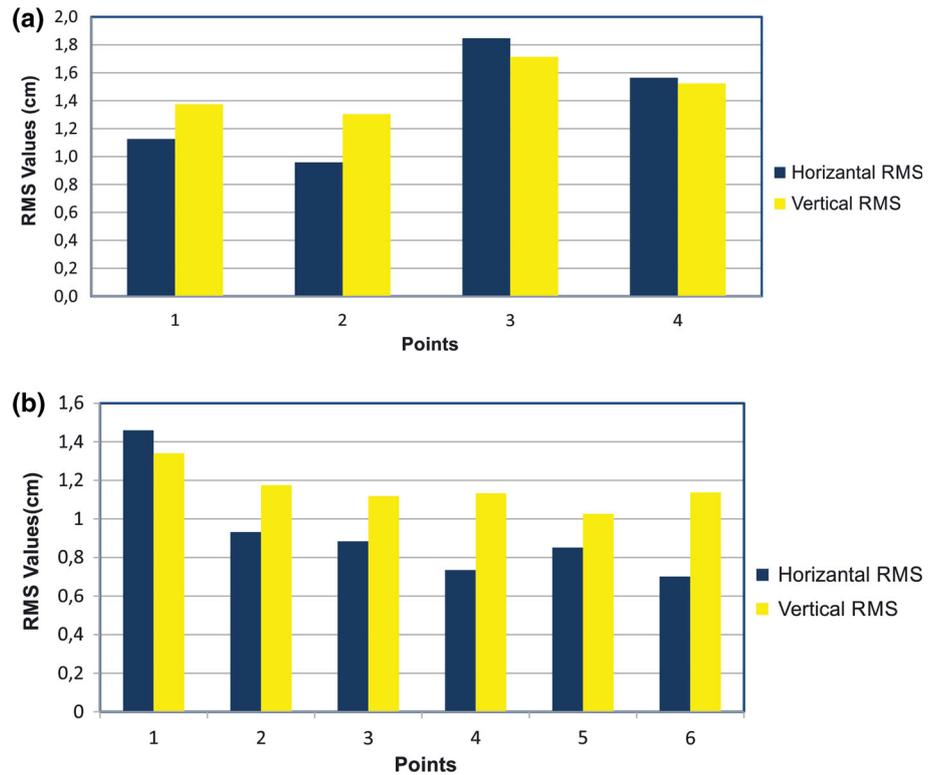

Fig. 7 GNSS integrated artificial target for geo-referencing

that displacements of more than 2 m had occurred. These findings indicate that the TLS data can be used in the analysis of displacements that have taken place or will take place in the future.

As shown in Table 1, the accuracy is close to 7 mm at a distance of 100 m. The accuracy of the TLS data and DTMs varies for two reasons. The first reason is associated with errors arising from the combination of TLS point clouds and errors caused by interpolation, which reduces the quality of the data. For example, the interpolation methods that are used may not always produce the desired accuracy. The other reason concerns objects that are not fixed on the topography. For example, the movement of plants on the terrain may produce a variation in topography. In this study, the errors in question (noise) were filtered using Geomagic software. Subsequent to these procedures, a DTM was obtained using Surfer Golden software v9 with a 5-cm grid interval (Fig. 8).

Global navigational satellite system monitoring

A mini geodetic network that included object (deformation points) and reference benchmarks was established for GNSS monitoring in the landslide area. The GNSS monitoring network in Taşkent includes four reference stations and nine rovers.

The master (reference) stations were located at geologically stable sites no more than a few kilometres from the rovers (short baselines).

Periodic GNSS monitoring consisted of rapid-static campaigns between November 2011 and April 2012. Surveys were performed with double-frequency receivers at the master stations and at the rovers simultaneously. Post-

Table 2 1st period geo-referencing results (in meters)

Maximum error	Minimum error		Mean error		Standard deviation	
0.029	0.021		0.025		0.005	
Source point (x)	Source point (y)	Source point (z)	Destination point (x)	Destination point (y)	Destination point (z)	Distance between centers
455,801.2,081	4,087,877.512	1,440.376	455,801.201	4,087,877.485	1,440.379	0.029
455,800.9,397	4,087,861.762	1,442.079	455,800.926	4,087,861.778	1,442.078	0.021
455,766.6,621	4,087,813.734	1,447.778	455,766.676	4,087,813.719	1,447.779	0.021
455,737.987	4,087,800.293	1,450.383	455,737.994	4,087,800.321	1,450.38	0.028

Table 3 2nd period geo-referencing results (in meters)

| Maximum Error	Minimum error		Mean error		Standard deviation	
0.044	0.011		0.032		0.012	
Source point (x)	Source point (y)	Source point (z)	Destination point (x)	Destination point (y)	Destination point (z)	Distance between centers
455,737.537	4,087,780.281	1,457.593	455,737.566	4,087,780.262	1,457.573	0.040
455,734.081	4,077,755.388	1,466.167	455,734.077	4,087,755.381	1,466.174	0.011
455,696.966	4,087,764.206	1,464.833	455,696.943	4,087,764.244	1,464.836	0.0444
455,725.602	4,087,715.891	1,480.596	455,725.609	4,087,715.907	1,480.621	0.031
455,691.669	4,087,716.369	1,482.735	455,691.638	4,087,716.366	1,482.724	0.034
455,697.716	4,087,666.446	1,503.964	455,697.738	4,087,666.421	1,503.959	0.0340
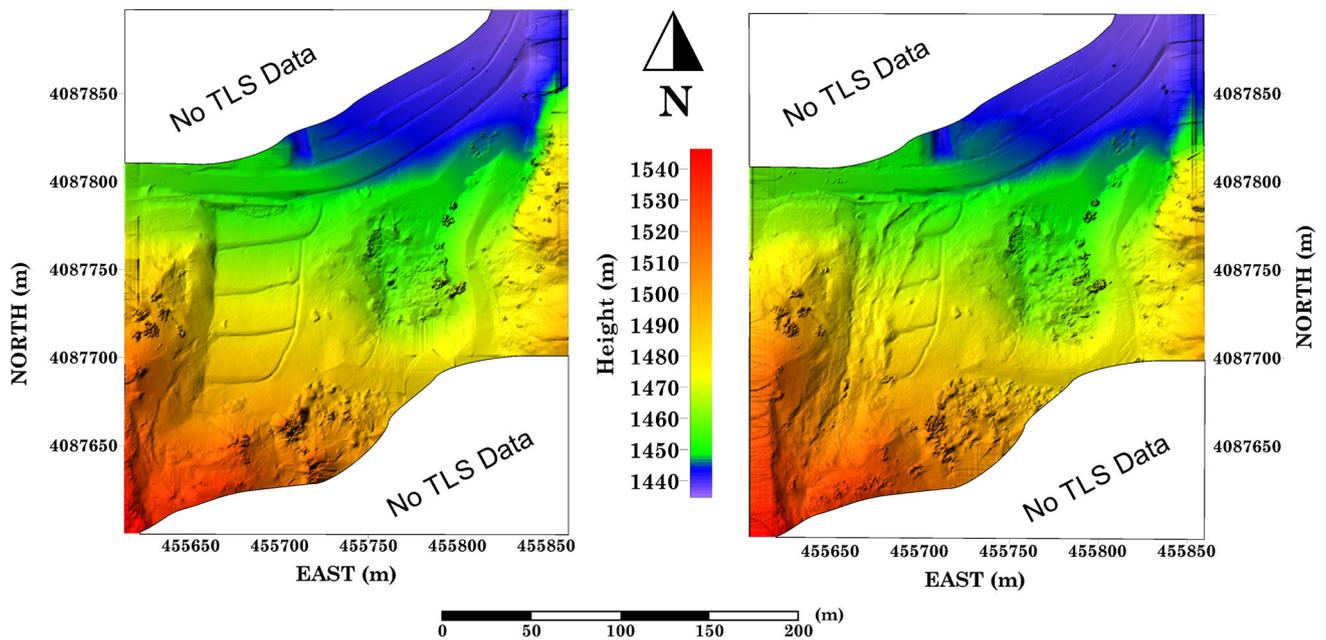
Fig. 8 a First period **b** second period digital terrain model with ITRF coordinate system

Table 4 Horizontal and vertical movement rapid-static GNSS analysis results

Point ID	Horizontal movements			Vertical movements
	ΔN (m)	ΔE (m)	Δ (m)	Δh (m)
GNSS1	–	–	–	–
GNSS2	0.824	0.140	0.836	−0.246
GNSS3	0.541	0.010	0.541	−0.145
GNSS4	–	–	–	–
GNSS5	0.200	−0.004	0.200	−0.103
GNSS6	–	–	–	–
GNSS7	0.900	0.002	0.900	−0.638
GNSS8	1.071	−0.014	1.071	−0.796
GNSS9	0.886	−0.051	0.887	−0.993

processing of surveys was executed with commercial software Leica GEO Office v5.

To determine movements with a static model, a functional model, solved according to the least-squares method, was constituted for each observation period.

The test statistic value computed from the difference vector and covariance matrix was compared with the *F*-distribution. As a result, moving points and movements were computed (Yalçinkaya and Bayrak 2005; Koch 1999).

Results

The results of rapid-static GNSS monitoring surveys showed a total displacement at the upper parts of the landslide ranging between 0.20 m and 1.00 m over five months. The precision obtained with the GNSS is within a few centimetres for rapid-static observations. However, the analysis of the field data demonstrates that the GNSS technique is not appropriate for monitoring areas of large mass movements.

In the study area, nine GNSS benchmarks were established for the detection of landslides, to estimate which areas had the potential for landslide occurrence. Three of these benchmarks were lost owing to the huge mass of landslide movement. The remaining benchmarks were evaluated for this study (Fig. 10).

On the basis of movements recorded by GNSS campaigns using six GNSS rovers, rovers GNSS1, GNSS4 and GNSS6 were destroyed by earthflow (Table 4).

The point cloud data can be evaluated using different methods: point cloud-point cloud comparisons, comparisons among DTMs, two-dimensional section comparisons and volume-related comparisons (Corsini et al. 2009; Monserrat and Crosetto 2008). In this study, all of the aforementioned comparison methods were used. The measurements performed, the data obtained and the results gathered through the comparison of the data in the landslide area are presented below.

Positive values (indicating swelling zones) and negative values (indicating depression zones) were obtained as a result of a comparison of point clouds belonging to different periods. These positive and negative values provide information about the movement of the points in the landslide area (Oppikofer et al. 2009). Comparisons made between the coordinates (*x*, *y* and *z*) reveal the changes that occurred along the axes. However, it is possible to determine the difference between the point clouds by finding the nearest point (Fig. 9). Employing this method, it is possible
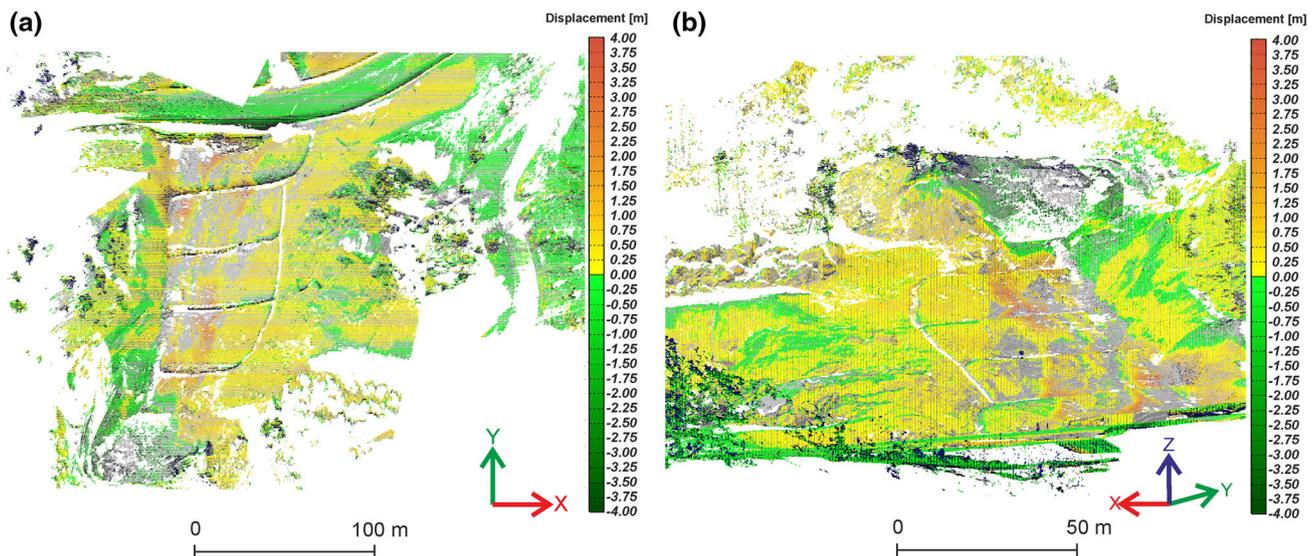

Fig. 9 *Grey* and *white areas* are those with no point data, so comparisons were not made in these areas. **a** Orthogonal view in point-to-point comparisons **b** perspective view

to obtain a difference factor consisting of the x, y and z coordinates of points belonging to two different periods. This is commonly done, especially when information about the direction of movement is available. However, this method has disadvantages. For example, because the shortest distance between two points is determined using this method, the results should be evaluated on a vector basis (Chen and Medioni 1991). There are numerous software programs that use the method (CloudCompare 2013; Geomagic 2012; Polyworks 2007). In this study, analyses were performed according to the shortest distance between points using the PolyWorks IMInspect module, and comparative images of point clouds belonging to the landslide area were obtained (Fig. 9). In these images, the depression and swelling values between the points are shown in shades of light green and a colour scale changing from yellow to red, respectively. As can be observed from an examination of these shapes, depressions and swellings ranging from –4 to 4 m were discovered in the landslide area. It is concluded that the method of point-to-point comparison can be effectively used in the detection of depressions and swellings in the landslide area. This finding is in accordance with the results obtained using the other comparative methods detailed below.

Point-to-point comparisons require point data in areas that will be compared. The comparison of points that do not have data is not possible through this method. To eliminate this situation, a DTM of the landscape was

generated using the point cloud data. In addition, changes in the land surface can be better observed when shaded relief maps are generated (Fig. 10).

A small grid interval was selected to obtain an appropriate landscape model (<0.5 m). Activities in the landscape area were monitored through a comparison of DTMs belonging to different periods (Fig. 8). As shown in Fig. 11, depressions of up to –4 m (blue areas) and swelling areas of up to 4 m (red areas) were detected using this method. It was also observed that swellings and depressions over the entire landscape generally varied by ±1.10 m (yellow and light-blue areas).

Software can facilitate 3D comparisons among DTMs. A 3D displacement model of the landscape area was obtained by comparing the DTMs that were generated using data obtained from the landscape area at two different times. The areas of depression, swelling and displacement were determined by an examination of these models. As a result of the 3D comparison, it was observed that depressions and swellings of up to 4 m occurred in the terrain and that swellings of 0–1.35 m generally occurred (Fig. 11).

Another comparison method used to study the landslide was the comparison of cross-sections taken from the area through a 3D model comparison. Six different cross-section drawings were made of the area through a DTM to compare two-dimensional cross-sections. The direction of slide in the landslide area and the directions orthogonal to
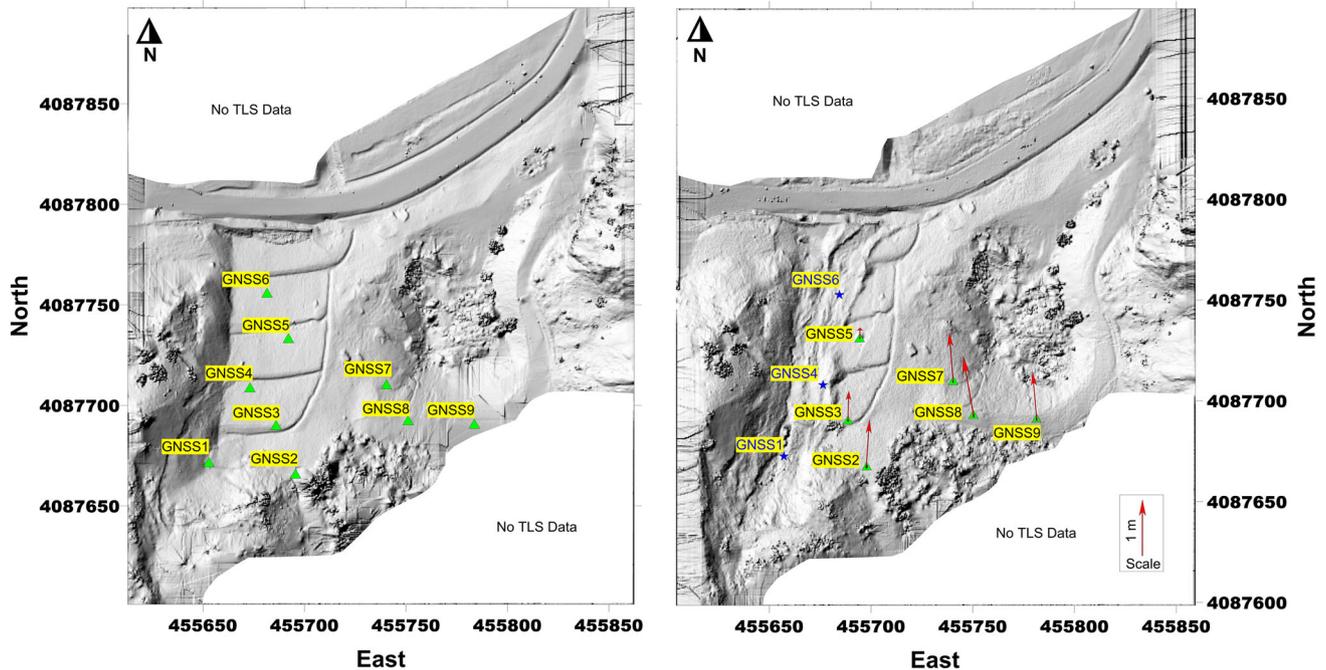

Fig. 10 *Shaded* relief map of the study area with GNSS benchmarks and their movements on horizontal blue star benchmarks are destroyed by landslide (*debris flow*): **a** first period shaded map and **b** second period shaded map

Fig. 11 3D Comparison of two different digital terrain models
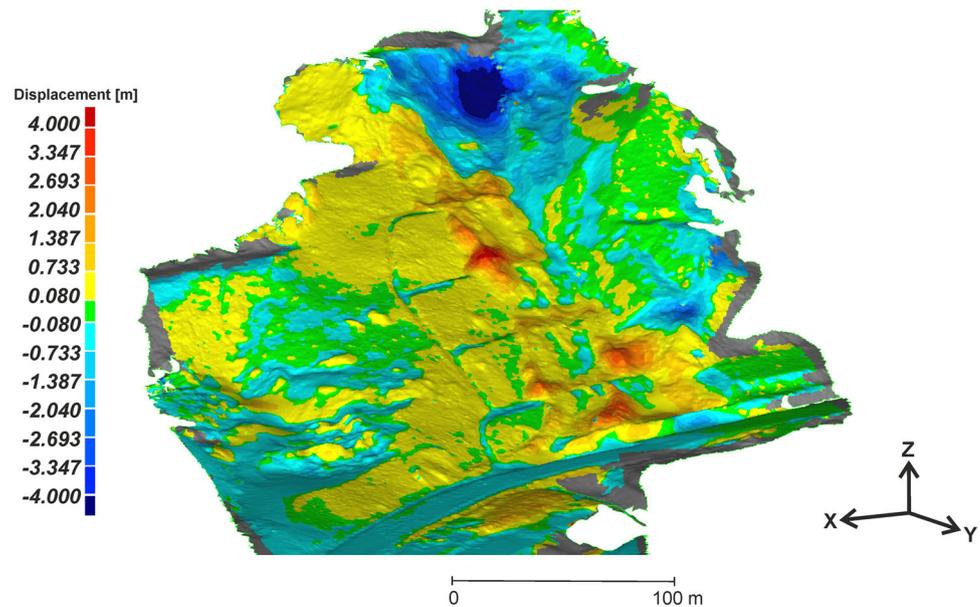
it were taken into consideration to determine the locations of the cross-sections. Moreover, an effort was made to have the cross-sections pass through areas where displacements in the landscape were the highest in number and the most visible. Four cross-sections (cross-sections a–a′, b–b′, c–c′, and d–d′) in the direction of the displacement and two cross-sections orthogonal to it (cross-sections e–e′ and f–f′) were created. The locations of these cross-sections are shown in Fig. 12. Displacement information regarding the relevant point between the reference surface (the surface obtained in the first period) and the test surface (the surface obtained in the second period) can be obtained with these cross-sections. The direction of movement was determined using the cross-section method. However, the difference between the DTMs in the profile cross-section indicates the amount of landslide movement. The colour representation of the deviation vectors in the cross-sections (based on their size) facilitated the evaluation. The deviation value belonging to any point on the cross-section can, thus, be determined.

As observed from an examination of the cross-sections, there were depressions of up to 4 m south of the landslide area (area of rupture), whereas there were swellings of up to 2.20 m in the north (area of accumulation) (Fig. 13b). This result is in agreement with the formations of depressions and swellings that are generally observed in landslide areas.

When the cross-sections are examined, ground movements approaching 4 m can be observed (a–a′ in Fig. 12). In the 3D model, a depression (on the Z axis) is generally observed in the upper and lower sections, whereas northward movements are observed in the middle section (on the Y axis).

Another method of evaluation involves cubing or volume calculations. Landslide movements that occur on the surface in a study area can also be determined using volume calculations (Pirotti et al. 2012; Syahmi et al. 2011). A discernible change in volume is observed between the two measurements. This situation can be visually verified in the 3D model that was obtained from the TLS data. However, it is important to quantitatively determine the volume (Tsakiri et al. 2006). Therefore, the difference in volume in the active area was calculated. Differences in volume between the first-period and second-period DTMs were determined to monitor the movements in the landslide area (Table 5). The dimensions of the area selected for volume calculation in the landslide area were 220 m (455,609–455,829) in the direction of X, 319 m (4,087,617–4,087,936) in the direction of Y and 107 m (1,431–1,538) in the direction of Z, with a surface area of 39,112 m^2. The volume of the DTM obtained in the first period on a certain plane was calculated, and the volume of the DTM obtained in the second period was then calculated. The difference between the volumes yielded the total change in volume in the landslide area. The change in volume that occurred in the area of study as a result of the slide was calculated to be 60,330 m^3. When this figure is divided by the surface of the study area, an average elevation of 1.5 is obtained. Displacements of up to 1.5 m, obtained as a result of volume comparisons, are in agreement with the values obtained from the surface comparisons (Fig. 11).

The occurrence of major deformations within a 5-month period indicates that this area is prone to frequent and sizeable landslides. The volume was calculated with the aid of a reference plane of known elevation, and the volume differences between the periods belonging to the same borders were determined. The volume changes resulting

from displacements in the landslide area were calculated through this analysis. Thus, it is clearly shown that the results of all of these comparisons and analysis are in agreement with one another.

Discussion

TLS devices allow for the rapid and accurate acquisition of millions of 3D data points from the surface of the Earth. These devices can be used over large areas and from long distances owing to their high accuracy in processing the measurement of distances.

Many studies in laser scanning technology are aimed at obtaining and processing data. In addition, TLS is effectively used in geological studies. The results of our study appear to support this assertion.

Our study demonstrated that better predictions can be made in landslide studies with highly accurate (7 mm at 100 m) and numerous ($\sim 51 \times 10^6$) point data. According

Fig. 13 Deviation values for Dx, Dy, and Dz, axes. D shows the total ▶ amount of deviation. The *colour scale* is the *coloured* state of amount D. **a–a′** is 455,645.00 cross-section in the direction of X (the amount and activity of the depression which occurred in the upper part of the land model was monitored). **b–b′** is 455,680.200 cross-section in the direction of X (watching the small hill that was formed in the middle by the earth flow coming from the upper part of the area). **c–c′** is 455,719.188 cross-section in the direction of X. **d–d′** is 455,750.200 cross-section in the direction of X. **e–e′** is 4,087,690.900 cross-section in the direction of Y. **f–f′** is 4,087,750.900 cross-section in the direction of Y

to Staiger (2003), although other devices and systems (for example, tachometers and laser radars) have higher accuracy than TLS devices (0.5 mm and 0.05 m, respectively), their measurement distance is short and their rate of data acquisition is low. Moreover, TLS is able to obtain millions of 3D points within minutes, which is nearly impossible using total stations. Airborne LiDAR methods and other satellite techniques can be applied in larger areas, but their accuracy and density of points are lower; i.e., 10–15 cm

Fig. 12 Locations of cross-sections in the digital terrain model
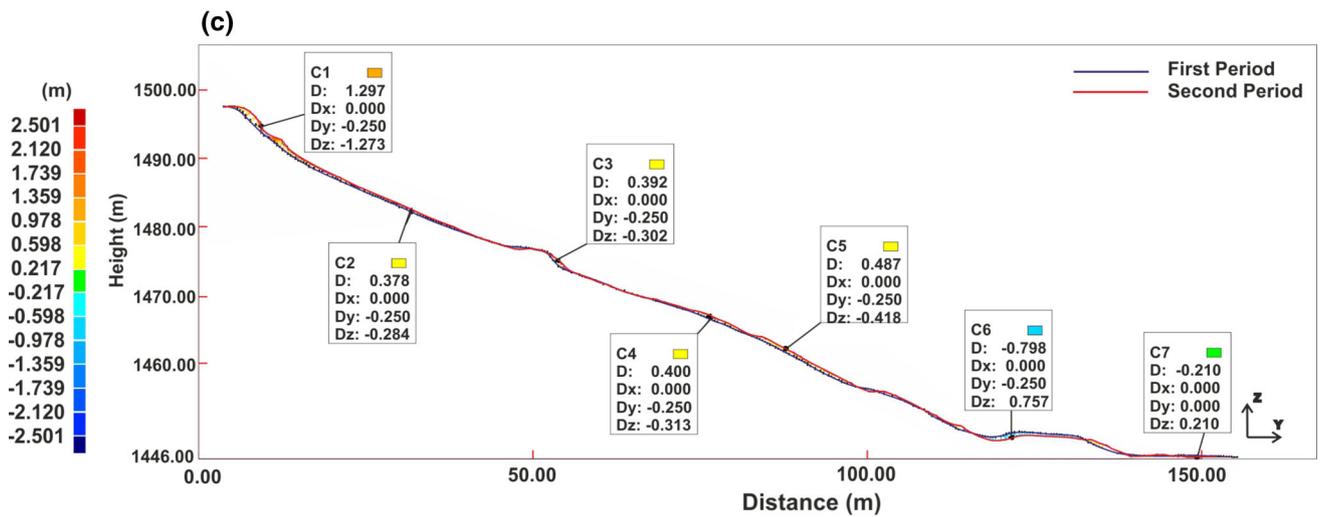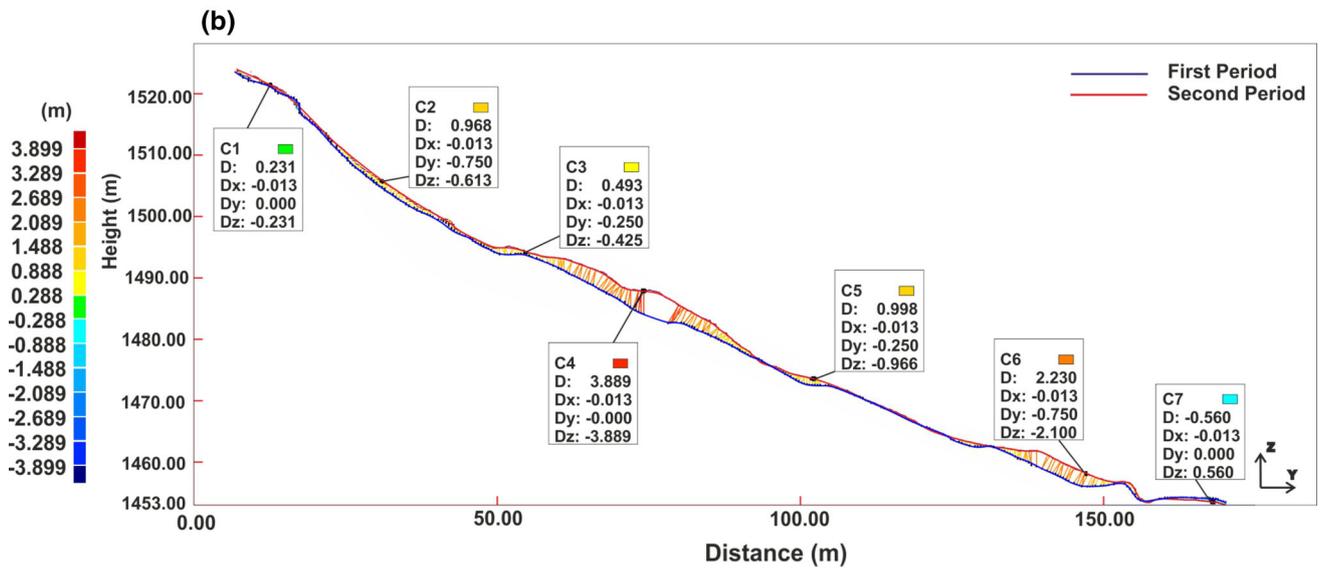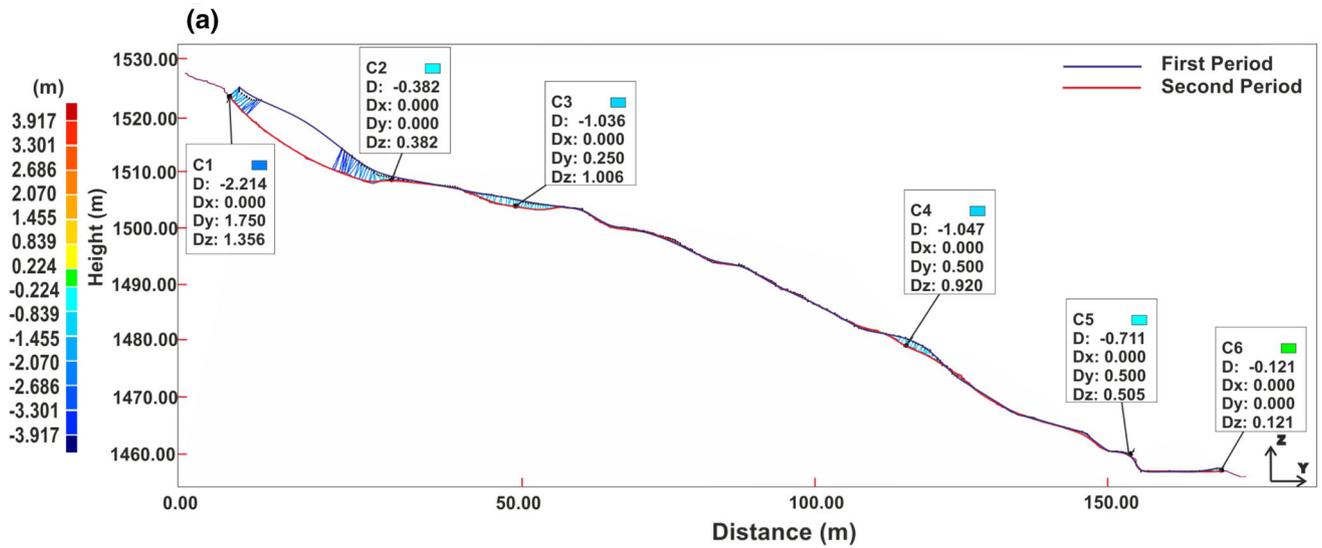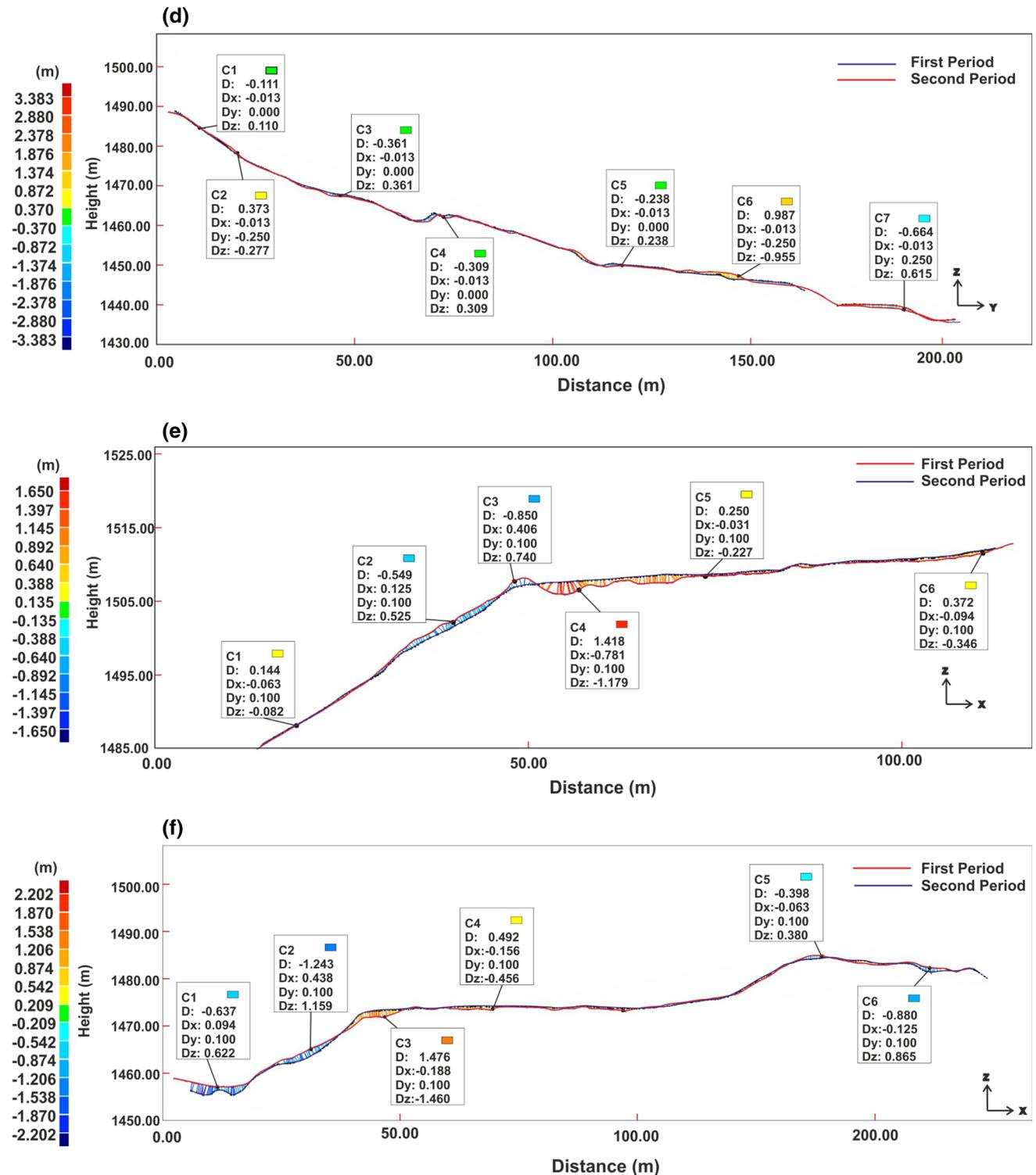
Fig. 13 continued

and 20 points/m², respectively (Cavalli and Marchi 2008; McKean and Roering 2004). Moreover, airborne LiDAR only offers a vertical view; it is difficult to obtain high accuracy for a stepped slope. Bitelli et al. (2004) and Demir et al. (2004) compared TLS and photogrammetric techniques and proposed that TLS should be the preferred alternative to photogrammetry and that DTMs could be obtained more accurately and at a lower cost. However, the

Table 5 Surface areas, volumes and differences

	Level of reference plane (m)	Surface area (m^2)	Volume (m^3)
1st period	1,400	55,837.350	3,351,850.018
2nd period	1,400	56,352.678	3,412,180.888
Difference	–	515.328	60,330.870

problem of shaded areas arises in each measurement. We encountered this problem with both techniques. This problem appears for high, flat and horizontal surfaces. However, the fact that the study area in the present study had a larger angle of gradient and that scans were performed in different fields of view allowed the terrestrial laser scan technique to be more productive, thus, obviating the need for aerial measurements. Moreover, the cost of airborne LiDAR is very high by Turkish standards. Although TLS can obtain data more quickly and can obtain more intensive data, processing these data poses a different problem. Future studies should ensure that data intensity is optimised in each scan. In short, the question of how many data points are needed to arrive at the most accurate result in the shortest time span must be solved.

Conclusions

In landslide monitoring studies, GNSS techniques produce highly accurate results. However, huge mass landslide movements can destroy or lose benchmarks, in which case the monitoring process is not able to continue. TLS techniques are more suitable in such situations because they do not depend on stable benchmarks in the landslide area. While the GNSS benchmarks were lost on site, TLS data aided in the assessment of the site. The biggest advantage of this technique is that the entire landslide area can be measured by means of laser technology. The study area can, thus, be further assessed. Therefore, TLS measurements have been shown to be more suitable for the monitoring of landslides of huge mass.

Long-distance TLS is a simple, fast and highly accurate method used for determining the geometrical characteristics of landslides that occur in large areas. This technology was used to examine the landslide that occurred in Taşkent. Gathering point clouds using ILRIS-3D is an effective and useful method for the acquisition of detailed inventories associated with high-accuracy 3D models and landslides. These 3D data have been effective in better understanding the geometric characteristics of land surfaces.

The direction, volume and characteristics of the landslide were obtained with high accuracy. The developments and calculations made in this study allowed for reliable predictions of the characteristics of the landslide that occurred in the area. TLS contributed positively to the examination of the landslide within a short time and at a low cost.

References

Abellán A, Vilaplana JM, Martínez J (2006) Application of a long-range terrestrial laser scanner to a detailed rockfall study at Vall de Núria (Eastern Pyrenees, Spain). Eng Geol 88(3–4):136–148. doi:10.1016/j.enggeo.2006.09.012

Besl PJ, McKay ND (1992) A method for registration of 3-D shapes. IEEE Trans Pattern Anal Mach Intell 14(2):239–256

Bitelli G, Dubbini M, Anutta A (2004) Terrestrial laser scanning and digital photogrammetry techniques to monitor landslide bodies. Paper presented at the XXth ISPRS. Commission V, WG V/2, Istanbul, Turkey

Brideau M-A, Sturzenegger M, Stead D, Jaboyedoff M, Lawrence M, Roberts NJ, Ward BC, Millard TH, Clague JJ (2012) Stability analysis of the 2007 Chehalis lake landslide based on long-range terrestrial photogrammetry and airborne LiDAR data. Landslides 9(1):75–91. doi:10.1007/s10346-011-0286-4

Bruckl E, Brunner FK, Kraus K (2006) Kinematics of a deep-seated landslide derived from photogrammetric. GPS and geophysical data. Eng Geol 88(3–4):149–159

Casula G, Mora P, Bianchi MG (2010) Detection of terrain morphologic features using GPS, TLS, and land surveys: "tana della volpe" blind valley case study. J Surv Eng ASCE 136(3):132–138. doi:10.1061/(asce)su.1943-5428.0000022

Cavalli M, Marchi L (2008) Characterisation of the surface morphology of an alpine alluvial fan using airborne LiDAR. Nat Hazard Earth Syst 8(2):323–333. doi:10.5194/nhess-8-323-2008

Chen Y, Medioni G (1991) Object modeling by registration of multiple range images. In: IEEE international conference on robot and automation, Sacramento

CloudCompare (2013) Telecom ParisTech (version 2.4) [GPL software]. EDF R&D

Corsini A, Borgatti L, Coren F, Vellico M (2007) Use of multitemporal airborne lidar surveys to analyse post-failure behaviour of earth slides. Can J Remote Sens 33(2):116–120. doi:10.5589/m07-015

Corsini A, Borgatti L, Cervi F, Dahne A, Ronchetti F, Sterzai P (2009) Estimating mass-wasting processes in active earth slides - earth flows with time-series of High-Resolution DEMs from photogrammetry and airborne LiDAR. Nat Hazard Earth Syst 9(2):433–439. doi:10.5194/nhess-9-433-2009

Daehne A, Corsini A (2013) Kinematics of active earthflows revealed by digital image correlation and DEM subtraction techniques applied to multi-temporal LiDAR data. Earth Surf Proc Land 38(6):640–654. doi:10.1002/esp.3351

Demir N, Bayram B, Alkış Z, Helvacı C, Çetin I, Vögtle T, Ringle K, Steinle E (2004) Laser scanning for terrestrial photogrammetry, alternative system or combined with traditional system. Paper presented at the proceeding of the XXth ISPRS commission V, WG V/2, Istanbul, Turkey, 12–23 July

Fanti R, Gigli G, Lombardi L, Tapete D, Canuti P (2012) Terrestrial laser scanning for rockfall stability analysis in the cultural heritage site of Pitigliano (Italy). Landslides 1–12. doi:10.1007/s10346-012-0329-5

Gallay M, Lloyd CD, McKinley J, Barry L (2013) Assessing modern ground survey methods and airborne laser scanning for digital terrain modelling: a case study from the Lake District, England. Comput Geosci 51:216–227. doi:10.1016/j.cageo.2012.08.015

Geomagic (2012) Software (Version 2012). Suite 300 Morrisville, NC 27560, USA

Ghuffar S, Szekely B, Roncat A, Pfeifer N (2013) Landslide displacement monitoring using 3D range flow on airborne and terrestrial LiDAR data. Remote Sens 5(6):2720–2745

Gigli G, Morelli S, Fornera S, Casagli N (2012) Terrestrial laser scanner and geomechanical surveys for the rapid evaluation of rock fall susceptibility scenarios. Landslides. doi:10.1007/s10346-012-0374-0

Gili JA, Corominas J, Rius J (2000) Using global positioning system techniques in landslide monitoring. Eng Geol 55(3):167–192

Gruen A, Akca D (2005) Least squares 3D surface and curve matching. ISPRS J Photogramm 59(3):151–174. doi:10.1016/j.isprsjprs.2005.02.006

Guarnieri A, Vettore A, Camarda M, Domenica C (2011) Automatic registration of large range datasets with spin-images. J Cult Herit 12(4):476–484

Guarnieri A, Milan N, Vettore A (2013) Monitoring of complex structure for structural control using terrestrial laser scanning (Tls) and photogrammetry. Int J Archit Herit 7(1):54–67

Heritage GL, Large ARG (2009) Laser scanning for the environmental sciences. Wiley-Blackwell. doi:10.1002/9781444311952

Kasperski J, Delacourt C, Allemand P, Potherat P, Jaud M, Varrel E (2010) Application of a terrestrial laser scanner (TLS) to the study of the Séchilienne landslide (Isère, France). Remote Sens 2(12):2785–2802. doi:10.3390/rs122785

Koch KR (1999) Parameter estimation and hypothesis testing in linear models. Springer-Verlag, Berlin

Kraus K (2007) Photogrammetry: geometry from images and laser scans (trans: Ian A. Harley, Kyle S). Walter de Gruyter, Germany

McKean J, Roering J (2004) Objective landslide detection and surface morphology mapping using high-resolution airborne laser altimetry. Geomorphology 57(3–4):331–351. doi:10.1016/s0169-555x(03)00164-8

Monserrat O, Crosetto M (2008) Deformation measurement using terrestrial laser scanning data and least squares 3D surface matching. ISPRS J Photogramm 63(1):142–154. doi:10.1016/j.isprsjprs.2007.07.008

Oppikofer T, Jaboyedoff M, Blikra L, Derron MH, Metzger R (2009) Characterization and monitoring of the Åknes rockslide using terrestrial laser scanning. Nat Hazard Earth Syst 9(3):1003–1019. doi:10.5194/nhess-9-1003-2009

Özgül N (1997) Bozkır-Hadim-Taşkent (Orta Toroslar'ın Kuzey Kesimi) Dolayında Yer Alan Tektono-Stratigrafik Birliklerin Stratigrafisi. MTA Dergisi 119:113–174 (in Turkish)

Pesci A, Teza G, Casula G, Loddo F, De Martino P, Dolce M, Obrizzo F, Pingue F (2011) Multitemporal laser scanner-based observation of the Mt. Vesuvius crater: characterization of overall geometry and recognition of landslide events. ISPRS J Photogramm 66(3):327–336

Pirotti F, Grigolato S, Lingua E, Sitzia T, Tarolli P (2012) Laser scanner applications in forest and environmental sciences. Ital J Remote Sens 44(1):109–123. doi:10.5721/Itjrs20124419

Polyworks (2007) Beginner's guide InnovMetric Software Inc. QC Canada

Ristic A, Abolmasov B, Govedarica M, Petrovacki D, Ristic A (2012) Shallow-landslide spatial structure interpretation using a multi-geophysical approach. Acta Geotech Slov 9(1):47–59

Staiger R (2003) Terrestrial laser scanning technology, systems and applications. In: 2nd FIG regional conference, Morocco

Syahmi MZ, Wan Aziz WA, Zulkarnaini MA, Anuar A, Othman Z (2011) The movement detection on the landslide surface by using terrestrial laser scanning. In: IEEE control and system graduate research colloquium (ICSGRC), Shah Alam, 27–28 June 2011, pp 175–180

Teza G, Galgaro A, Zaltron N, Genevois R (2007) Terrestrial laser scanner to detect landslide displacement fields: a new approach. Int J Remote Sens 28(16):3425–3446. doi:10.1080/01431160601024234

Teza G, Atzeni C, Balzani M, Galgaro A, Galvani G, Genevois R, Luzi G, Mecatti D, Noferini L, Pieraccini M, Silvano S, Uccelli F, Zaltron N (2008a) Ground-based monitoring of high-risk landslides through joint use of laser scanner and interferometric radar. Int J Remote Sens 29(16):4735–4756. doi:10.1080/01431160801942227

Teza G, Pesci A, Genevois R, Galgaro A (2008b) Characterization of landslide ground surface kinematics from terrestrial laser scanning and strain field computation. Geomorphology 97(3–4):424–437. doi:10.1016/j.geomorph.2007.09.003

Travelletti J, Malet JP, Samyn K, Grandjean G, Jaboyedoff M (2011) Control of landslide retrogression by discontinuities: evidence by the integration of airborne- and ground-based geophysical information. Landslides 10(1):37–54. doi:10.1007/s10346-011-0310-8

Travelletti J, Malet JP, Samyn K, Grandjean G, Jaboyedoff M (2013) Control of landslide retrogression by discontinuities: evidence by the integration of airborne- and ground-based geophysical information. Landslides 10(1):37–54

Tsakiri M, Lichti D, Pfeifer N (2006) Terrestrial laser scanning for deformation monitoring. In: 3rd IAG/12th FIG symposium, Baden, 22–24 May 2006

Turan A (2000) Korualan ve Bağbaşı (Hadim-Konya) Arasındaki Bölgenin Yapısal Özellikleri. DEÜ Mühendislik Fakültesi Fen ve Mühendislik Dergisi 2(3):51–65 (in Turkish)

Viero A, Furlanis S, Squarzoni C, Teza G, Galgaro A, Gianolla P (2012) Dynamics and mass balance of the 2007 Cima Una rockfall (Eastern Alps, Italy). Landslides. doi:10.1007/s10346-012-0338-4

Wang G, Philips D, Joyce J, Rivera F (2011) The integration of TLS and continuous GPS to study landslide deformation: a case study in Puerto Rico. J Geodetic Sci 1(1):191–203. doi:10.2478/v10156-010-0004-5

Yalçinkaya M, Bayrak T (2005) Comparison of static, kinematic and dynamic geodetic deformation models for Kutlugün landslide in northeastern Turkey. Nat Hazards 34(1):91–110. doi:10.1007/s11069-004-1967-2